Journal of Sound and Vibration 328 (2009) 57–70

Contents lists available at ScienceDirect

Journal of Sound and Vibration

journal homepage: www.elsevier.com/locate/jsvi

The vibrational properties of a periodic composite pipe in 3D space

Huijie Shen, Jihong Wen, Dianlong Yu, Xisen Wen *

Institute of Mechanical Engineering, and the PBG Research Center, National University of Defense Technology, Changsha 410073, China

ARTICLE INFO

Article history:
Received 19 May 2009
Received in revised form
18 July 2009
Accepted 30 July 2009
Handling Editor: L.G. Tham
Available online 21 August 2009

ABSTRACT

Piping system vibrations exist in many fields. Vibration control is very important because it can limit possible damage to pipe systems caused by vibrations. Applying the idea of the Bragg scattering mechanism of phononic crystals (PCs), a pipe is designed as a periodic composite material structure. Using the transfer matrix method, the band structure of an infinite periodic straight pipe structure is calculated. With knowledge of the vibration band gaps, a 3D space pipe system is designed with a composite material periodic structure, and its various vibration modes' frequency response functions are calculated. The accuracy of the transfer matrix method is verified with the commercial software MSC.Actran. The results show that the Bragg band gaps still exist in the 3D periodic pipe structure, and vibrations are strongly attenuated within the frequency ranges of the band gaps. Using the idea of PCs in piping systems provides a novel way to reduce pipe vibration.

1. Introduction

Piping systems have wide applications to areas such as designing heat exchanger tubes in chemical plants, main steam pipes and hot/cold leg pipes in nuclear steam supply systems, oil pipelines, pump discharge lines, marine risers, etc. [1]. Inevitably, as the piping systems work, undesirable noise and vibrations are produced. The vibration not only emits noise pollution but would also lead to a piping system surge, slow down the circulate reliability of system, deteriorate the work environment or even paralyze the pipe system and machines. Therefore, the piping system vibration control makes great sense for engineering applications and an extensive effort has been made in the analysis of the piping system vibrations [1–8].

In the last decade, the propagation of elastic or acoustic waves in periodic composite materials called phononic crystals (PCs) has received considerable attention [9–18]. The emphasis of these studies was focused on the existence of complete elastic band gaps within which both sound and vibration are forbidden. There are two kinds of band gap formation in PCs: the Bragg scattering mechanism and the locally resonant (LR) mechanism [19]. The most important characteristic of a PC is its periodic structure [19]. Periodically engineered structures, such as railway lines on equi-spaced sleepers, antenna systems, stiffened plates used in aircraft and ship panels, and truss structures on space stations have special characteristics of free wave propagation with wave blocking and wave propagation frequency bands [2].

Studies have shown that the existence of Bragg gaps is strongly connected with large acoustic impedance between the scatterers and the matrix material [19]. For PCs with band gaps induced by the Bragg scattering mechanism, their band gap frequency ranges are wide. Furthermore, within this band gap frequency range, vibration wave propagation is strongly attenuated.

* Corresponding author. Tel./fax: +86 731 4574975.
E-mail address: wenxs@vip.sina.com (X. Wen).

0022-460X/$ - see front matter © 2009 Elsevier Ltd. All rights reserved.
doi:10.1016/j.jsv.2009.07.032

Sorokin modeled a straight pipe wall as a periodic cylindrical shell structure to determine the band gaps. Based on Floquet theory, Sorokin analyzed the energy transmission in compound cylindrical shell periodic structures [3]. Yu Dianlong et al. introduced the Bragg scattering mechanism and LR mechanism respectively into the straight pipe's structure design, and obtain corresponding band structure, and studied the flexural vibration wave propagation properties within the band gaps [20]. There are many vibrational modes that exist in piping systems, such as longitudinal vibration, flexural vibration, torsional vibration, and coupled vibration modes. To our knowledge, no work appears in the open literature studying the coupled vibration properties of a 3D periodic pipe system.

In this paper, we base the design of a composite material pipe with a periodic structure on the Bragg scattering mechanism of PCs. Using the transfer matrix (TM) method, we calculate the flexural vibration, longitudinal vibration, and torsional vibration band gaps of an infinite straight periodic structure. Furthermore, we design a 3D piping system composed of composite materials with a periodic structure and study its vibration transfer properties. In the FRF calculation, we use the TM method, which is validated using the commercial software MSC.Actran. The frequency response functions (FRFs) of the coupled mode vibration are calculated to investigate the coupled mode vibration band gaps properties of the straight finite periodic pipe. Using the idea of PCs, the Bragg scattering mechanism, and a periodic pipe structure with vibration band gaps, we provide a new way to control vibrations in piping systems.

2. Pipe model and motion equations

For piping systems, in which the inside diameter of the pipe is much smaller than the pipe length, usually be calculated based on Timoshenko beam model or Euler beam model [21]. The Euler beam equations do not take into consideration the shear distortion and section moment of inertia. In order to calculate the flexural vibration FRF more accurately, in this paper, we base our calculations on the Timoshenko beam model. Fig. 1 shows the straight periodic pipe structure designed based on the Bragg scattering mechanism of PCs. Pipe A with length a_1 and pipe B with length a_2 repeatedly alternate along the axial direction. Thus, the PC has a lattice constant of $a = a_1+a_2$. Pipes A and B are made up of different materials, *A* and *B*, or different geometrical parameters, respectively.

Fig. 2 shows the deformations and internal forces on a single pipe element for transfer vibration. In this paper, the pipe wall is assumed to be linearly elastic, isotropic, prismatic, circular, and thin-walled, which implies that the longitudinal

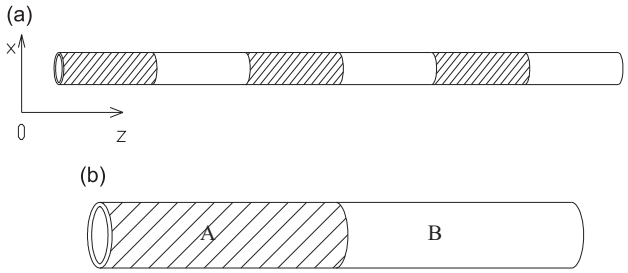

Fig. 1. The sketch map of periodic pipe structure. (a) Infinite periodic pipe structure and (b) Single pipe cell.

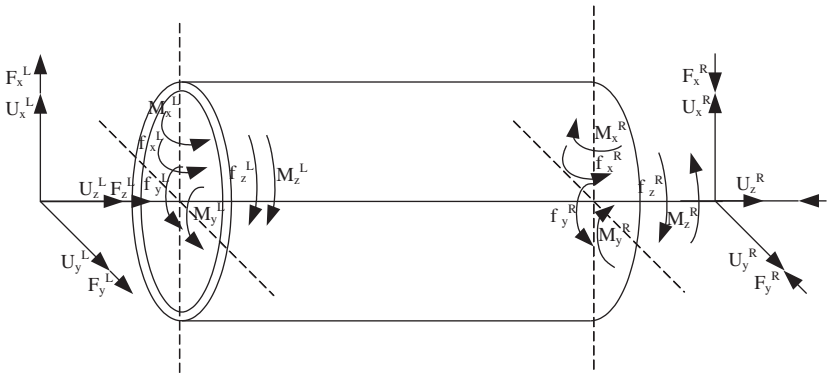

Fig. 2. Deformations and internal forces for transfer vibration of a single pipe element.

vibration of the pipe without fluid loading can be given as follows [21]:

$$\frac{\partial f_z}{\partial z} - A_p \rho_p \frac{\partial^2 u_z}{\partial t^2} = 0, \tag{1}$$

$$f_z - EA_p \frac{\partial u_z}{\partial z} = 0, \tag{2}$$

where f_z is the axial force, u_z is the pipe wall displacement in the axial direction, A_p is the cross-section area, ρ_p is the material density of pipe wall, E is Young's modulus (considering that the damp modulus of material, E, can be written as $E(1+\mathrm{i}\eta)$, where η is the damp modulus of the material), and t is the time.

For flexural vibration, the motion equations are given as follows [21]:

$$f_x - GA_p k_s \left(\frac{\partial u_x}{\partial z} - \varphi_y \right) = 0, \tag{3}$$

$$m_y - EI_p \frac{\partial \varphi_y}{\partial z} = 0, \tag{4}$$

$$\frac{\partial f_x}{\partial z} - \rho_p A_p \frac{\partial^2 u_x}{\partial t^2} = 0, \tag{5}$$

$$\frac{\partial m_y}{\partial z} + f_x - \rho_p I_p \frac{\partial^2 \varphi_y}{\partial t^2} = 0, \tag{6}$$

where f_x is the pipe cross-section shear force, u_x is the displacement along the x-axis, φ_y is the cross-section slope, m_y is the bending moment, I_p is the moment of inertia of the pipe, A_p is the cross-section area of the pipe, G is the shear modulus, and $k_s = 2(1+\nu)/(4+3\nu)$ is the cross-section geometry shape parameter, $\nu = E/(2G) - 1$ is Poisson's ratio.

The torsional vibration is defined as [21]

$$\frac{\partial m_z}{\partial z} - \rho_p J_p \frac{\partial^2 \psi_z}{\partial t^2} = 0, \tag{7}$$

$$m_z - GJ_p \frac{\partial \psi_z}{\partial z} = 0, \tag{8}$$

where m_z is internal moment, ψ_z is the rotation in the axis direction, and J_p is the polar moment of inertia for the pipe wall.

3. The TM method for band structure and the FRF of a straight pipe

3.1. Longitudinal vibration state vector

For a given oscillatory frequency, ω, the solution of Eqs. (1) and (2) can be written in the form: $f_z(z,t) = F_z(z)\mathrm{e}^{\mathrm{j}\omega t}$ and $u_z(z,t) = U_z(z)\mathrm{e}^{\mathrm{j}\omega t}$, where $j = (-1)^{1/2}$ and $F_z(z)$ and $U_z(z)$ are defined as

$$U_z(z) = A_1 \mathrm{e}^{\mathrm{j}\lambda z} + A_2 \mathrm{e}^{-\mathrm{j}\lambda z}, \tag{9}$$

$$F_z(z) = \mathrm{i}EA_p\lambda A_1 \mathrm{e}^{\mathrm{j}\lambda z} - \mathrm{i}EA_p\lambda A_2 \mathrm{e}^{-\mathrm{j}\lambda z}, \tag{10}$$

where $\lambda = \omega\sqrt{\rho_p/E}$.

Eqs. (9) and (10) can be written in matrix form as follows:

$$\begin{bmatrix} U_z(z) \\ F_z(z) \end{bmatrix} = \begin{bmatrix} \mathrm{e}^{\mathrm{j}\lambda z} & \mathrm{e}^{-\mathrm{j}\lambda z} \\ \mathrm{i}EA_p\lambda \mathrm{e}^{\mathrm{j}\lambda z} & -\mathrm{i}EA_p\lambda \mathrm{e}^{-\mathrm{j}\lambda z} \end{bmatrix} \begin{bmatrix} A_1 \\ A_2 \end{bmatrix}, \tag{11}$$

which can be rewritten as

$$\boldsymbol{P}_{\mathrm{axial}} = \boldsymbol{T}_{\mathrm{axial}} \cdot \boldsymbol{A}. \tag{12}$$

3.2. Flexural vibration state vector in x–z plane

From Eqs. (3)–(6), we obtain

$$EI_p \frac{\partial^4 f_x}{\partial z^4} + \rho_p A_p \frac{\partial^2 f_x}{\partial t^2} - \rho_p I_p \frac{\partial^4 f_x}{\partial z^2 \partial t^2} + \frac{EI_p}{GA_p k_s} \frac{\partial^2}{\partial z^2} \left(\rho_p A_p + \frac{\partial^2 f_x}{\partial t^2} \right) + \frac{\rho_p A_p}{GA_p k_s} \frac{\partial^2}{\partial t^2} \left(\rho_p A_p \frac{\partial^2 f_x}{\partial t^2} \right) = 0. \tag{13}$$

For a given oscillatory frequency, ω, the solution of $f_x(z,t)$ can be written as $f_x(z,t) = F_x(z)e^{j\omega t}$, which can then be substituted into Eq. (11) to obtain:

$$F_x(z) = A_1 e^{\lambda_1 z/l} + A_2 e^{-\lambda_1 z/l} + A_3 e^{j\lambda_2 z/l} + A_4 e^{-j\lambda_2 z/l}, \tag{14}$$

where

$$\lambda_{1,2} = \sqrt{\sqrt{\gamma + \frac{1}{4}(\sigma-\tau)^2} \mp \frac{(\sigma+\tau)}{2}}, \quad \sigma = \frac{\rho_p A_p}{G A_p \kappa_s}\omega^2 l^2, \ \gamma = \frac{\rho_p A_p}{E I_p}\omega^2 l^4,$$

and $l = a_1$ or a_2.

Further, $u_x(z,t)$, $\varphi_y(z,t)$, and $m_y(z,t)$ can be written as $u_x(z,t) = U_x(z)e^{j\omega t}$, $\varphi_y(z,t) = \Psi(z)e^{j\omega t}$, and $m_y(z,t) = M_y(z)e^{j\omega t}$, and these equations can be substituted into Eqs. (3)–(6) to obtain

$$U_x(z) = \frac{-l^3\lambda_1}{EI_p\gamma}(A_1 e^{\lambda_1 z/l} - A_2 e^{-\lambda_1 z/l}) + \frac{-l^3\lambda_2}{EI_p\gamma}(jA_3 e^{j\lambda_2 z/l} - jA_4 e^{-j\lambda_2 z/l}), \tag{15}$$

$$\Psi_y(z) = \frac{-l^2(\sigma+\lambda_1^2)}{EI_p\gamma}(A_1 e^{\lambda_1 z/l} + A_2 e^{-\lambda_1 z/l}) + \frac{-l^2(\sigma+\lambda_2^2)}{EI_p\gamma}(A_3 e^{j\lambda_2 z/l} + A_4 e^{-j\lambda_2 z/l}), \tag{16}$$

$$M_y(z) = \frac{-l(\sigma+\lambda_1^2)\lambda_1}{\gamma}(A_1 e^{\lambda_1 z/l} - A_2 e^{-\lambda_1 z/l}) + \frac{-l(\sigma+\lambda_2^2)\lambda_2}{\gamma}(-jA_3 e^{j\lambda_2 z/l} + jA_4 e^{-j\lambda_2 z/l}). \tag{17}$$

Eqs. (14)–(17) can be rewritten in matrix form

$$\begin{bmatrix} U_x(z) \\ \Psi_y(z) \\ M_y(z) \\ F_x(z) \end{bmatrix} = \begin{bmatrix} B_1 e^{\lambda_1 z/l} & -B_1 e^{-\lambda_1 z/l} & jB_2 e^{j\lambda_2 z/l} & -jB_2 e^{-j\lambda_2 z/l} \\ B_3 e^{\lambda_1 z/l} & B_3 e^{-\lambda_1 z/l} & B_4 e^{j\lambda_2 z/l} & B_4 e^{-j\lambda_2 z/l} \\ B_5 e^{\lambda_1 z/l} & -B_5 e^{-\lambda_1 z/l} & -jB_6 e^{j\lambda_2 z/l} & jB_6 e^{-j\lambda_2 z/l} \\ e^{\lambda_1 z/l} & e^{-\lambda_1 z/l} & e^{j\lambda_2 z/l} & e^{-j\lambda_2 z/l} \end{bmatrix} \begin{bmatrix} A_1 \\ A_2 \\ A_3 \\ A_4 \end{bmatrix}, \tag{18}$$

where

$$B_1 = \frac{-l^3}{EI_p\gamma}\lambda_1, \quad B_2 = \frac{-l^3}{EI_p\gamma}\lambda_2, \quad B_3 = \frac{-l^2}{EI_p\gamma}(\sigma+\lambda_1^2), \quad B_4 = \frac{-l^2}{EI_p\gamma}(\sigma-\lambda_2^2),$$

$$B_5 = \frac{-l}{\gamma}(\sigma+\lambda_1^2)\lambda_1 \quad \text{and} \quad B_6 = \frac{-l}{\gamma}(-\sigma+\lambda_2^2)\lambda_2.$$

The matrix in Eq. (18) can be rewritten in a shortened form

$$\boldsymbol{P}_{\text{flex}-xz} = \boldsymbol{T}_{\text{flex}-xz} \cdot \boldsymbol{B}. \tag{19}$$

The flexural vibration in the y–z plane can be written as follows:

$$\begin{bmatrix} U_y(z) \\ \Psi_x(z) \\ M_x(z) \\ F_y(z) \end{bmatrix} = \begin{bmatrix} B_1 e^{\lambda_1 z/l} & -B_1 e^{-\lambda_1 z/l} & jB_2 e^{j\lambda_2 z/l} & -jB_2 e^{-j\lambda_2 z/l} \\ B_3 e^{\lambda_1 z/l} & B_3 e^{-\lambda_1 z/l} & B_4 e^{j\lambda_2 z/l} & B_4 e^{-j\lambda_2 z/l} \\ B_5 e^{\lambda_1 z/l} & -B_5 e^{-\lambda_1 z/l} & -jB_6 e^{j\lambda_2 z/l} & jB_6 e^{-j\lambda_2 z/l} \\ e^{\lambda_1 z/l} & e^{-\lambda_1 z/l} & e^{j\lambda_2 z/l} & e^{-j\lambda_2 z/l} \end{bmatrix} \begin{bmatrix} A_1 \\ A_2 \\ A_3 \\ A_4 \end{bmatrix}, \tag{20}$$

where B_1, B_2, B_3, B_4, B_5, and B_6 are the same as the flexural vibration in the x–z plane. Again, the matrix in Eq. (20) can be rewritten in short form

$$\boldsymbol{P}_{\text{flex}-yz} = \boldsymbol{T}_{\text{flex}-yz} \cdot \boldsymbol{C}. \tag{21}$$

3.3. Torsional vibration state vector

The solutions of Eqs. (7) and (8) can be expressed as

$$\begin{bmatrix} \Psi_z(z) \\ M_z(z) \end{bmatrix} = \begin{bmatrix} \frac{\lambda}{\rho_p J_p l}\sin(\lambda\frac{z}{l}) & \frac{-\lambda}{\rho_p J_p l}\cos(\lambda\frac{z}{l}) \\ \cos(\lambda\frac{z}{l}) & \sin(\lambda\frac{z}{l}) \end{bmatrix} \begin{bmatrix} A_1 \\ A_2 \end{bmatrix}, \tag{22}$$

where $\lambda = \pm\omega l(\rho_p/G)^{1/2}$, which can be rewritten as follows:

$$\boldsymbol{P}_{\text{torsion}} = \boldsymbol{T}_{\text{torsion}} \cdot \boldsymbol{D}. \tag{23}$$

3.4. Band structure and FRFs

The pipe vibration state vector can be expressed as

$$\boldsymbol{Z}_{\text{straight}}(z) = \boldsymbol{T}_{\text{straight}} \cdot \boldsymbol{W}, \tag{24}$$

where

$$\boldsymbol{Z}_{\text{straight}}(z) = [\boldsymbol{P}_{\text{axial}} \ \boldsymbol{P}_{\text{flex}-xz} \ \boldsymbol{P}_{\text{flex}-yz} \ \boldsymbol{P}_{\text{torsion}}]'$$

$$\boldsymbol{T}_{\text{straight}} = \begin{bmatrix} \boldsymbol{T}_{\text{axial}} & & & \\ & \boldsymbol{T}_{\text{flex}-xz} & & \\ & & \boldsymbol{T}_{\text{flex}-yz} & \\ & & & \boldsymbol{T}_{\text{torsion}} \end{bmatrix},$$

and $\boldsymbol{W} = [\boldsymbol{A} \ \boldsymbol{B} \ \boldsymbol{C} \ \boldsymbol{D}]'$. The left and right state vector of pipe A in the nth cell as shown in Fig. 1 can be expressed as follows:

$$\boldsymbol{Z}^{L,R}_{nA\_s} = \boldsymbol{T}^{L,R}_{A\_s} \cdot \boldsymbol{W}_{nA}, \tag{25}$$

and for pipe B

$$\boldsymbol{Z}^{L,R}_{nB\_s} = \boldsymbol{T}^{L,R}_{B\_s} \cdot \boldsymbol{W}_{nB}. \tag{26}$$

The continuities of displacement, slope, bending moment, shear force, and axial force at the interfaces between cell $n-1$ and cell n, gives:

$$\boldsymbol{Z}^{R}_{(n-1)A\_s} = \boldsymbol{Z}^{L}_{(n-1)B\_s}, \tag{27}$$

$$\boldsymbol{Z}^{R}_{(n-1)B\_s} = \boldsymbol{Z}^{L}_{nA\_s}. \tag{28}$$

From Eqs. (25)–(28), we obtain

$$\boldsymbol{Z}^{R}_{nA} = \boldsymbol{T}^{R}_{A\_s} \cdot (\boldsymbol{T}^{L}_{A\_s})^{-1} \cdot \boldsymbol{Z}^{L}_{nA}, \tag{29}$$

$$\boldsymbol{Z}^{R}_{nB} = \boldsymbol{T}^{R}_{B\_s} \cdot (\boldsymbol{T}^{L}_{B\_s})^{-1} \cdot \boldsymbol{Z}^{L}_{nB}, \tag{30}$$

$$\boldsymbol{Z}^{L}_{nA} = \boldsymbol{T}^{R}_{B\_s} \cdot (\boldsymbol{T}^{L}_{B\_s})^{-1} \cdot \boldsymbol{T}^{R}_{A\_s} \cdot (\boldsymbol{T}^{L}_{A\_s})^{-1} \cdot \boldsymbol{Z}^{L}_{(n-1)A}. \tag{31}$$

Therefore, the transfer matrix in the straight periodic pipe is given as

$$\boldsymbol{T}_{s\_\text{cell}A} = \boldsymbol{T}^{R}_{A\_s} \cdot (\boldsymbol{T}^{L}_{A\_s})^{-1}, \tag{32}$$

$$\boldsymbol{T}_{s\_\text{cell}B} = \boldsymbol{T}^{R}_{B\_s} \cdot (\boldsymbol{T}^{L}_{B\_s})^{-1}, \tag{33}$$

$$\boldsymbol{T}_{s\_\text{cell}} = \boldsymbol{T}^{R}_{B\_s} \cdot (\boldsymbol{T}^{L}_{B\_s})^{-1} \cdot \boldsymbol{T}^{R}_{A\_s} \cdot (\boldsymbol{T}^{L}_{A\_s})^{-1}. \tag{34}$$

Due to the periodicity of the infinite structure in the axial direction, and in order to satisfy the Bloch theorem, we then get

$$\boldsymbol{Z}_{nA} = \mathrm{e}^{\mathrm{j}ka}\boldsymbol{Z}_{(n-1)A}, \tag{35}$$

where k is the 1D wave vector in the z direction. It follows that the eigenvalues of the infinite periodic pipe structure are the roots of the determinant:

$$|\boldsymbol{T}_{s\_\text{cell}} - \mathrm{e}^{\mathrm{j}ka}\boldsymbol{I}| = 0, \tag{36}$$

where I is the 12×12 unit matrix. For given values of ω, Eq. (36) gives the values of k. Depending on whether k is real or has an imaginary part, the corresponding wave propagates through the pipe (pass band) or is damped (band gap).

For a finite periodic structure, we can calculate the frequency response curve to describe its transfer property of band gaps. When the pipe consists of m periodic cells, we get

$$\boldsymbol{Z}_{(n+m)A} = \boldsymbol{T}^{m}_{s\_\text{cell}}\boldsymbol{Z}_{nA}. \tag{37}$$

4. Band structures and the coupled vibration FRFs calculation of the straight periodic pipe

For the periodic straight pipe shown in Fig. 1, we calculate the band structures assuming that the pipe material for pipe A is epoxy and that for pipe B is steel. The density, Young's modulus, and shear modulus of epoxy are $1180\,\text{kg}\,\text{m}^{-3}$,

0.435×10^{10} Pa, and 0.159×10^{10} Pa, whereas these values for steel are 7780 kg m^{-3}, 21.60×10^{10} Pa, and 8.10×10^{10} Pa. The lattice constant of the straight periodic pipe is chosen to be $a = 1$ m, and $a_1 = a_2 = 0.5$ m. The inner and outer radii of the pipe are chosen as $r_i = 0.09$ m and $r_o = 0.1$ m.

Fig. 3 shows the longitudinal vibration band structure of the periodic straight pipe. From Fig. 3, we can find that there are two band gaps between 0 and 3500 Hz. The band gap frequency ranges are 462–1876 and 2017–3700 Hz. Within the longitudinal vibration band gap frequency ranges, the propagation of longitudinal vibration waves is forbidden. Fig. 4 shows the flexural vibration band structure of the periodic straight pipe. From Fig. 4, it can be seen that there are seven band gaps between 0 and 3500 Hz. These gaps occur between 81 and 91 Hz, 289.4 and 613.2 Hz, 766.8 and 1246 Hz, 1414.7 and 1844.5 Hz, 2156.9 and 2185 Hz, 2473.8 and 3001.2 Hz, and 3117.8 and 3500 Hz. Within these band gap frequency ranges, the propagation of flexural vibration waves is forbidden. Fig. 5 shows the torsional vibration band structure for the periodic straight pipe. There were four band gaps in Fig. 5 between 0 and 3500 Hz, 279.5 and 1135.9 Hz, 1220.3 and 2244.1 Hz, 2340.1 and 3055.2 Hz, and 3261.2 and 3477.5 Hz. From Fig. 5, it can be seen that the torsional vibration band gap ranges are much wider and attenuation is stronger. If a kind of the three type wave excitation frequency were within the band gaps frequency ranges, the straight periodic pipe would lack any vibration.

Observing the band structures of Figs. 3–5, it can be seen that there are six overlapping band gaps frequency ranges between 0 and 3500 Hz, specifically at 462–613.2 Hz, 1220.3–1246 Hz, 1414.7–1844.5 Hz, 2156.9–2185.9 Hz, 2473.8–3001.2 Hz, and 3261.2–3477.5 Hz. Within these frequency ranges, the propagation of the longitudinal vibration,

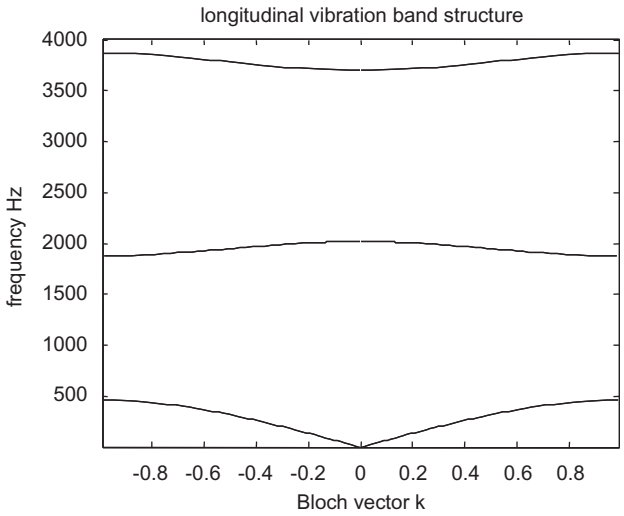

Fig. 3. The longitudinal vibration band structure of periodic straight pipe.

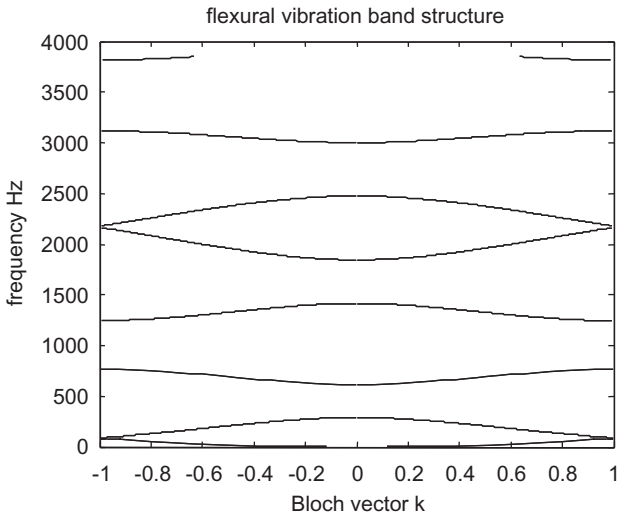

Fig. 4. The flexural vibration band structure of periodic straight pipe.

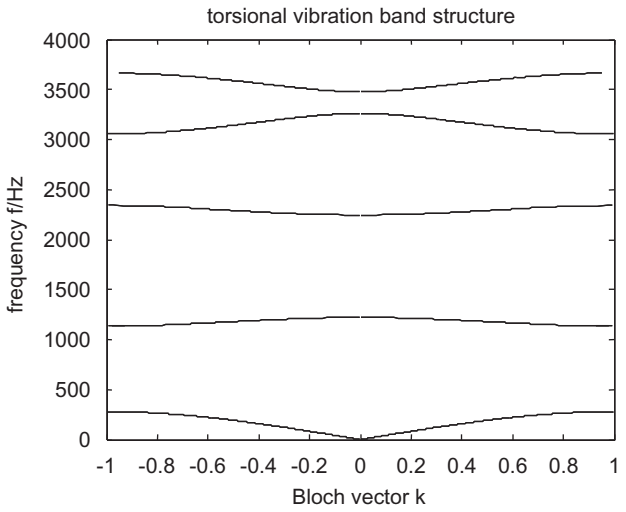

Fig. 5. The torsional vibration band structure of periodic straight pipe.

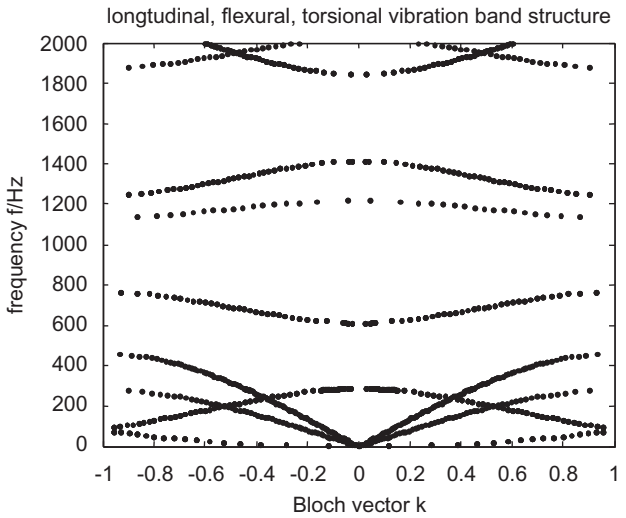

Fig. 6. The longitudinal, flexural and torsional vibration band structure of the periodic straight pipe.

flexural vibration, torsional vibration, and their coupled modes is forbidden. Fig. 6 shows the three types vibration band structure of the periodic straight pipe. The frequency ranges of the band gaps in Fig. 6 is just the overlapping band gaps frequency ranges of Figs. 3–5. In a straight pipe, the flexural vibration wave, longitudinal vibration wave, and torsional vibration wave can propagate individually. However, in the 3D pipe system, the wave energy which transfers among any types of the three wave types would result in model coupling vibration during propagation, for example, when the flexural wave propagates in the 3D periodic pipe, it could result in longitudinal vibration and torsional vibration. But in the periodic straight pipe, the propagation of flexural wave will not result in longitudinal and torsional vibration. And the pipe vibration would become complex and the band gaps would be different in the 3D pipe system. We will discuss it in the next section.

5. The FRFs of a 3D periodic pipe

Enlightened by the vibration reduction properties within the band gaps of the straight periodic pipe, we designed a 3D pipe into a periodic structure as shown in Fig. 7. The pipe is composed of periodic straight pipes and curved pipes, and the curved pipes are elbows or bent pipes with a constant curvature.

The pipe structure in Fig. 7 is the basic component section of a complex piping system. Therefore, understanding the vibration properties of this system is an important factor in complex piping system vibration reduction. The elbows in Fig. 7

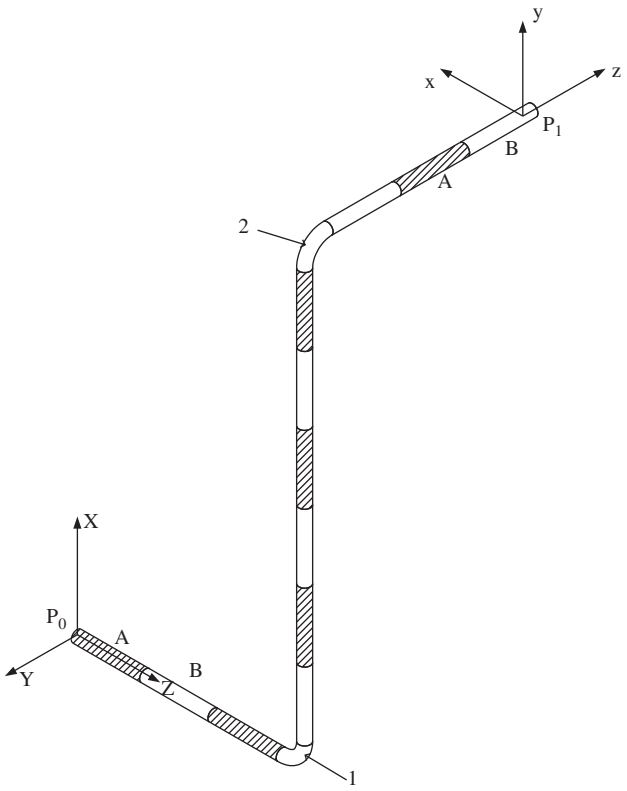

Fig. 7. The sketch map of a 3D periodic pipe.

can be treated as a collection of straight pipe sections [20], differing in orientation and joined end-to-end. Taking the elbow in the x–z plane, for example, suppose an elbow with a curvature radius, R, and angle, θ, and dividing it into m straight pipe sections, we then can use the small straight pipes joined end-to-end to model the elbow as shown in Fig. 8(a).

From the equilibrium of pipe forces, bending moment, and the continuity of pipe displacement and rotation at the bend point as shown in Fig. 8(b), we can obtain

$$\begin{bmatrix} U_z^R \\ F_z^R \\ U_x^R \\ M_y^R \\ \Psi_y^R \\ F_x^R \end{bmatrix} = \begin{bmatrix} \cos\alpha & 0 & \sin\alpha & 0 & 0 & 0 \\ 0 & \cos\alpha & 0 & 0 & 0 & \sin\alpha \\ -\sin\alpha & 0 & \cos\alpha & 0 & 0 & 0 \\ 0 & 0 & 0 & 1 & 0 & 0 \\ 0 & 0 & 0 & 0 & 1 & 0 \\ 0 & -\sin\alpha & 0 & 0 & 0 & \cos\alpha \end{bmatrix} \begin{bmatrix} U_z^L \\ F_z^L \\ U_x^L \\ M_y^L \\ \Psi_y^L \\ F_x^L \end{bmatrix}, \tag{38}$$

which can be denoted as

$$\boldsymbol{Z}_{cxz}^R = \boldsymbol{T}_{cxz}(\alpha) \cdot \boldsymbol{Z}_{cxz}^L. \tag{39}$$

And from the equilibrium of pipe forces, bending moment, and the continuity of pipe displacement and rotation at the bend point as shown in Fig. 8(c), we can obtain

$$\begin{bmatrix} U_y^R \\ F_y^R \\ \Psi_x^R \\ \Psi_z^R \\ M_x^R \\ M_z^R \end{bmatrix} = \begin{bmatrix} 1 & 0 & 0 & 0 & 0 & 0 \\ 0 & 1 & 0 & 0 & 0 & 0 \\ 0 & 0 & \cos\alpha & -\sin\alpha & 0 & 0 \\ 0 & 0 & \sin\alpha & \cos\alpha & 0 & 0 \\ 0 & 0 & 0 & 0 & \cos\alpha & -\sin\alpha \\ 0 & 0 & 0 & 0 & \sin\alpha & \cos\alpha \end{bmatrix} \begin{bmatrix} U_y^L \\ F_y^L \\ \Psi_x^L \\ \Psi_z^L \\ M_x^L \\ M_z^L \end{bmatrix}, \tag{40}$$

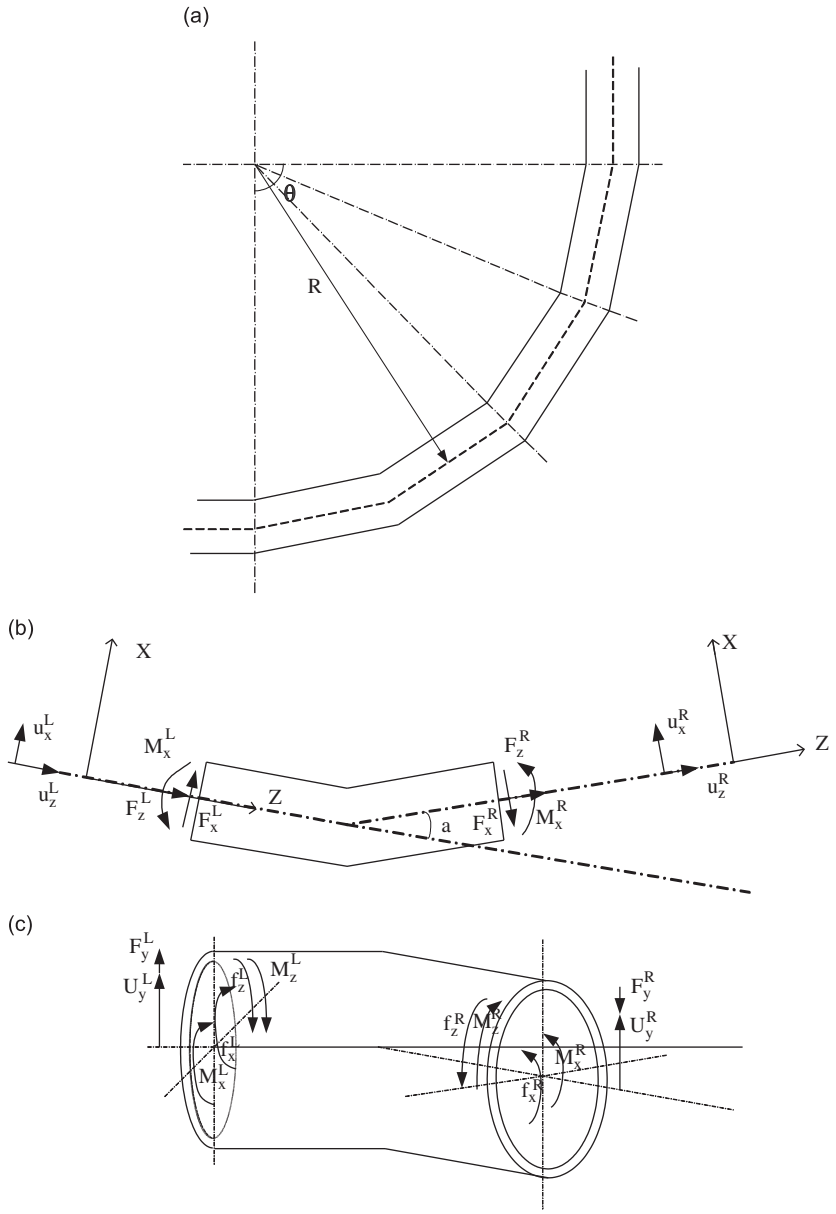

Fig. 8. (a) The sketch of a pipe bend consisted of a collection of straight pipes reaches. (b) Force and displacement at a single bend point in $x-z$ plane. (c) Force and displacement at a single bend point in the 3D space.

which can be denoted as

$$\boldsymbol{Z}_{cyz}^{R} = \boldsymbol{T}_{cyz}(\alpha) \cdot \boldsymbol{Z}_{cyz}^{L}. \tag{41}$$

Eqs. (37) and (39) can be composed as

$$\boldsymbol{Z}_{c1}^{R} = \boldsymbol{T}_{cs1}(\alpha) \cdot \boldsymbol{Z}_{c1}^{L}, \tag{42}$$

where

$$\boldsymbol{Z}_{c1} = [\boldsymbol{Z}_{cxz}\ \ \boldsymbol{Z}_{cyz}]', \quad \boldsymbol{T}_{cs1}(\alpha) = \begin{bmatrix} \boldsymbol{T}_{cxz}(\alpha) & \\ & \boldsymbol{T}_{cyz}(\alpha) \end{bmatrix}, \quad \alpha = \theta/m.$$

Then, the vibration transfer matrix of the elbow in the x–z plane is denoted as

$$\boldsymbol{T}_{c1} = \boldsymbol{T}_{cs1}(\alpha/2) \cdot \boldsymbol{T}_{cs1}(\alpha)^{m-1} \cdot \boldsymbol{T}_{cs1}(\alpha/2). \tag{43}$$

In order to research the global vibration transfer property of the 3D periodic pipe, we use the chain rule in the FRF calculation. The straight pipe vibration state vector and the curved pipe vibration state vector can be rearranged in a uniform form

$$\boldsymbol{Z}_g = [U_X(z)\ U_y(z)\ U_z(z)\ F_x(z)\ F_y(z)\ F_z(z)\ \Psi_x(z)\ \Psi_y(z)\ \Psi_z(z)\ M_x(z)\ [M_y(z)\ M_z(z)]'. \tag{44}$$

To make the transfer matrix compatible with the state vector, Z_g, the columns and rows of the matrices in Eqs. (32)–(34) and (43) must be rearranged. The straight pipe transfer matrix can be rearranged by a square matrix, t_s, and the curved pipe in the x–z plane can be rearranged by a square matrix, t_{c1}. The transfer matrix in the y–z plane can be obtained by exchanging the subscript x and y of the curved pipe state vector in the x–z plane and rearranging its corresponding transfer matrix in the x–z plane. This can be carried out by a square matrix, t_{c2}. The square matrices are given in Appendix.

At this point, the vibration transfer property of the 3D periodic pipe as shown in Fig. 7 is

$$\boldsymbol{Z}_{P_1} = \boldsymbol{T}_{gs\_cell} \cdot \boldsymbol{T}_{gs\_cellA} \cdot \boldsymbol{T}_{gc2} \cdot \boldsymbol{T}_{gs\_cellB} \cdot \boldsymbol{T}_{gs\_cell}^2 \cdot \boldsymbol{T}_{gs\_cellA} \cdot \boldsymbol{T}_{gc1} \cdot \boldsymbol{T}_{gs\_cellB} \cdot \boldsymbol{T}_{gs\_cell} \cdot \boldsymbol{Z}_{P_0} \tag{45}$$

The inner and outer radii and materials are chosen to be the same as the periodic straight pipe. The curvature angle and curvature radius of the elbow are chosen as: $\theta = 90^\circ$ and $R = 0.1$ m, respectively, and the material of the elbow is steel. Figs. 9–11 show the FRFs of the longitudinal, flexural, and torsional component vibration in a coupled mode vibration, respectively, of the 3D periodic pipe shown in Fig. 7. The dashed and solid lines in Figs. 9–11 correspond to the TM method calculation and the MSC.Actran calculation, respectively. From these figures, it can be seen that the TM calculation agrees very well with the MSC.Actran calculation; however, the results do not agree as well as the straight periodic pipe because of the accumulation of error caused by the TM method in calculating complex pipe systems. It should also be noted that the frequency ranges are nearly identical.

Comparing Fig. 3 with Fig. 9, Fig. 4 with Fig. 10, and Fig. 5 with Fig. 11, it can be seen that the longitudinal vibration band gaps, the flexural vibration band gaps and the torsional vibration band gaps of the 3D periodic pipe is much as the same as the band gaps of straight periodic pipe. And the corresponding types of vibration would be attenuated strongly within its band gaps frequency ranges. This effectively illuminates the advantage of applying the idea of PCs along with the Bragg scattering mechanism to pipe wall design to control piping system vibration. However, in the 3D pipe system, the wave energy which transfers among any types of elastic wave would result in model coupling vibration during propagation, therefore, the coupled mode vibration FRF should be calculated the investigate the vibration properties of the 3D periodic pipe system.

Fig. 12 shows the FRFs of different wave excitation of the 3D periodic pipe. The solid, dashed and dash dotted lines are corresponding to the flexural wave excitation, longitudinal wave excitation, and the coupled mode wave excitation of flexural, longitudinal and torsional waves. Observing the solid line in Fig. 12, we can find that there are four band gaps, they are: 260–340 Hz, 380–610 Hz, 780–1150 Hz and 1415–1745 Hz. There are three band gaps occurred in the dashed line, they are: 260–610 Hz, 750–1180 Hz, and 1400–1780 Hz. And three band gaps in the coupled mode vibration, they are: 265–610 Hz, 750–1180 Hz, and 1380–1780 Hz. By now, we can find that the frequency ranges of the real band gaps of the 3D periodic pipe system change little as the change of different wave type loads. Comparing the band gaps in Fig. 12 with the band gaps in Fig. 6, we can find that no matter how the load case changed, the center frequency and frequency ranges of the second and third band gaps are approximately the same as the band gaps in Fig. 6. That is because the frequency ranges of the second and third band gap are the overlapped frequency ranges of longitudinal vibration, flexural vibration and torsional vibration band gaps. Change much of the band gap frequency range is the first band gap. Observing the first band

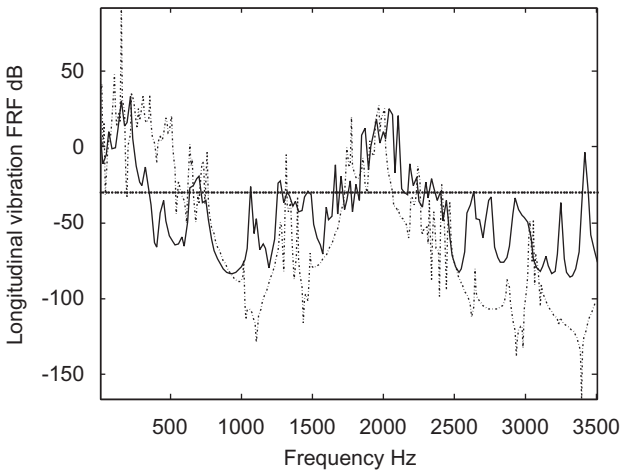

Fig. 9. The FRF of the longitudinal vibration component in the coupled mode vibration of the 3D periodic pipe, the solid and dashed lines are corresponding the MSC and the TM calculation, respectively.

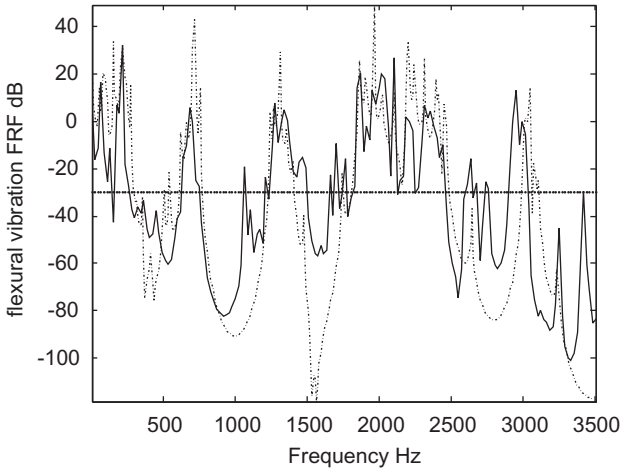

Fig. 10. The FRF of the flexural vibration component in the coupled mode vibration of the 3D periodic pipe, the solid and dashed lines are corresponding the MSC and the TM calculation, respectively.

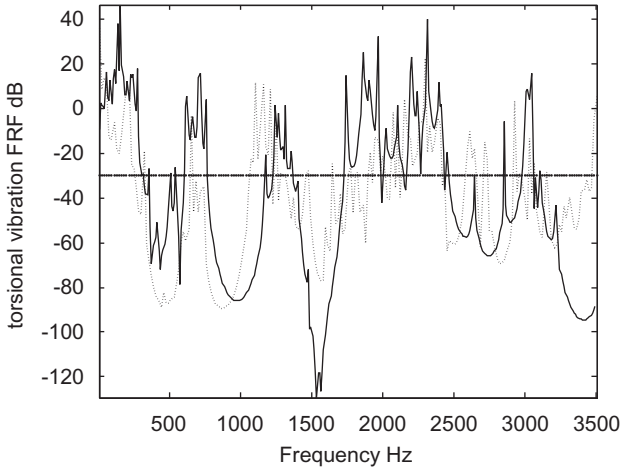

Fig. 11. The FRF of the torsional vibration component in the coupled mode vibration of the 3D periodic pipe, the solid and dashed lines are corresponding the MSC and the TM calculation, respectively.

gap in Fig. 6, we can find that between 0 and 450 Hz, there are no band gaps. However, there are overlapped frequency ranges of the first band gaps between Figs. 3 and 4, Figs. 3 and 5, Figs. 4 and 5. Between 0 and 450 Hz of the FRFs in Fig. 12, there appear band gaps, and this might be the coupled effect of the flexural vibration, longitudinal vibration and torsional vibration. With the changed of different wave excitation, the flexural vibration ingredient, longitudinal ingredient and torsional component will be changed, and that could affect the coupling mode of the 3D periodic pipe system, therefore, the first band gaps of the FRFs of the 3D periodic pipe system will changed as the load case changed.

6. Conclusion

In this paper, based on the Bragg scattering mechanism of PCs, we designed a pipe constructed with a composite material periodic structure. Using the TM method, we calculated the band structure of the flexural vibration, longitudinal vibration, and torsional vibration band gaps of an infinite periodic structure. The results show that the vibration band gaps attenuate vibrations effectively. From these results, we designed a 3D piping system with a composite material periodic structure and studied its vibration transfer properties. The results show that the 3D periodic piping system still demonstrates Bragg band gaps, and within these band gaps' frequency ranges, vibration could be strongly attenuated. The vibration-attenuating effect of this periodic pipe provides a novel way for vibration control in complex piping systems.

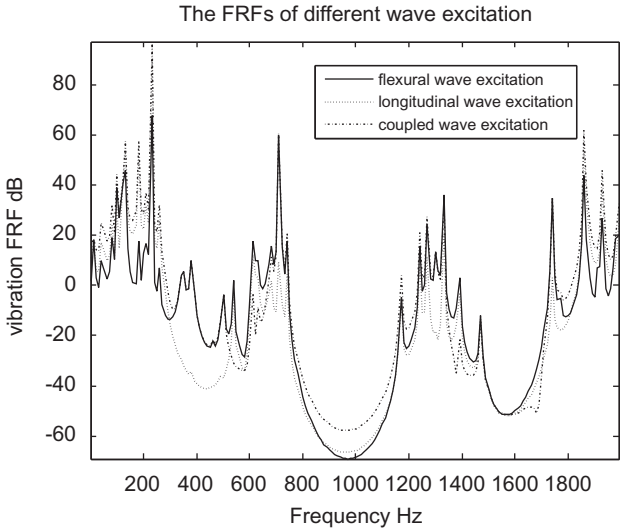

Fig. 12. The FRFs of the different wave excitation of the 3D periodic pipe.

Acknowledgment

This work was funded by the National Natural Science Foundation of China (Grant no. 50875255).

Appendix. The location exchange rule of pipe vibration state vector

To make the pipe vibration compatible with the chain rule, the columns and rows of the transfer matrices must be rearranged. First, the unaltered straight pipe vibration state vector is given as:

$$\boldsymbol{Z}_{\text{straight}} = [U_z(z)\ F_z(z)\ U_x(z)\ \Psi_y(z)\ M_y(z)\ F_x(z)\ U_y(z)\ \Psi_x(z)\ M_x(z)\ F_y(z)\ \Psi_z(z)\ M_z(z)]'.$$

The uniform pipe vibration state, Z_g, is given as

$$\boldsymbol{Z}_g = [U_x(z)\ U_y(z)\ U_z(z)\ F_x(z)\ F_y(z)\ F_z(z)\ \Psi_x(z)\ \Psi_y(z)\ \Psi_z(z)\ M_x(z)\ M_y(z)\ M_z(z)]'.$$

Comparing the state vectors in $\boldsymbol{Z}_{\text{straight}}$ and $\boldsymbol{Z}_g$, it can be seen that, for example, the third element, $U_x(z)$, is now the first, and the seventh element, $U_y(z)$, is now the second. In a similar manner, the transfer matrix is rearranged. Row and column shifting can be achieved in two steps: (i) the columns are rearranged by postmultiplying the transfer matrix, t_s; (ii) the rearrangement of rows is accomplished by premultiplying by t_s^t. The straight pipe transfer matrixes, $\boldsymbol{T}_{s\_\text{cell}}$, $\boldsymbol{T}_{s\_\text{cell}A}$, and $\boldsymbol{T}_{s\_\text{cell}B}$ in Eqs. (32)–(34),are rearranged as $\boldsymbol{T}_{gs\_\text{cell}}$, $\boldsymbol{T}_{gs\_\text{cell}A}$, and $\boldsymbol{T}_{gs\_\text{cell}B}$; where $\boldsymbol{T}_{gs\_\text{cell}} = t_s^t \cdot \boldsymbol{T}_{s\_\text{cell}} \cdot t_s$, $\boldsymbol{T}_{gs\_\text{cell}A} = t_s^t \cdot \boldsymbol{T}_{s\_\text{cell}A} \cdot t_s$, and $\boldsymbol{T}_{gs\_\text{cell}B} = t_s^t \cdot \boldsymbol{T}_{s\_\text{cell}B} \cdot t_s$. Further, t_s is given by

$$t_s = \begin{bmatrix} 0&0&1&0&0&0&0&0&0&0&0&0 \\ 0&0&0&0&0&0&1&0&0&0&0&0 \\ 1&0&0&0&0&0&0&0&0&0&0&0 \\ 0&0&0&0&0&1&0&0&0&0&0&0 \\ 0&0&0&0&0&0&0&0&0&1&0&0 \\ 0&1&0&0&0&0&0&0&0&0&0&0 \\ 0&0&0&0&0&0&0&1&0&0&0&0 \\ 0&0&0&1&0&0&0&0&0&0&0&0 \\ 0&0&0&0&0&0&0&0&0&0&1&0 \\ 0&0&0&0&0&0&0&0&1&0&0&0 \\ 0&0&0&0&1&0&0&0&0&0&0&0 \\ 0&0&0&0&0&0&0&0&0&0&0&1 \end{bmatrix}.$$

The previous curved pipe vibration state vector in the x–z plane is given as

$$\boldsymbol{Z}_{c1} = [U_z(z)\ F_z(z)\ U_x(z)\ M_y(z)\ \Psi_y(z)\ F_x(z)\ U_y(z)\ F_y(z)\ \Psi_x(z)\ \Psi_{x(z)}\ M_z(z)]'.$$

Rearranging this to be in the uniform state vector form, $\boldsymbol{Z}_g$, using the above method for the straight pipe, the transfer matrix of the curved pipe becomes $\boldsymbol{T}_{gc1}$, and $\boldsymbol{T}_{gc1} = t_{c1}^t \cdot \boldsymbol{T}_{c1} \cdot t_{c1}$, where

$$t_{c1} = \begin{bmatrix} 0 & 0 & 1 & 0 & 0 & 0 & 0 & 0 & 0 & 0 & 0 & 0 \\ 0 & 0 & 0 & 0 & 0 & 0 & 1 & 0 & 0 & 0 & 0 & 0 \\ 1 & 0 & 0 & 0 & 0 & 0 & 0 & 0 & 0 & 0 & 0 & 0 \\ 0 & 0 & 0 & 0 & 0 & 1 & 0 & 0 & 0 & 0 & 0 & 0 \\ 0 & 0 & 0 & 0 & 0 & 0 & 0 & 1 & 0 & 0 & 0 & 0 \\ 0 & 1 & 0 & 0 & 0 & 0 & 0 & 0 & 0 & 0 & 0 & 0 \\ 0 & 0 & 0 & 0 & 0 & 0 & 0 & 0 & 1 & 0 & 0 & 0 \\ 0 & 0 & 0 & 0 & 1 & 0 & 0 & 0 & 0 & 0 & 0 & 0 \\ 0 & 0 & 0 & 0 & 0 & 0 & 0 & 0 & 0 & 1 & 0 & 0 \\ 0 & 0 & 0 & 0 & 0 & 0 & 0 & 0 & 0 & 0 & 1 & 0 \\ 0 & 0 & 0 & 1 & 0 & 0 & 0 & 0 & 0 & 0 & 0 & 0 \\ 0 & 0 & 0 & 0 & 0 & 0 & 0 & 0 & 0 & 0 & 0 & 1 \end{bmatrix}.$$

Furthermore, the transfer matrix of the curved pipe in the $y-z$ plane is $\boldsymbol{T}_{gc2} = t_{c2}^t \cdot \boldsymbol{T}_{gc1} \cdot t_{c2}$, where

$$t_{c2} = \begin{bmatrix} 0 & 1 & 0 & 0 & 0 & 0 & 0 & 0 & 0 & 0 & 0 & 0 \\ 1 & 0 & 0 & 0 & 0 & 0 & 0 & 0 & 0 & 0 & 0 & 0 \\ 0 & 0 & 1 & 0 & 0 & 0 & 0 & 0 & 0 & 0 & 0 & 0 \\ 0 & 0 & 0 & 0 & 1 & 0 & 0 & 0 & 0 & 0 & 0 & 0 \\ 0 & 0 & 0 & 1 & 0 & 0 & 0 & 0 & 0 & 0 & 0 & 0 \\ 0 & 0 & 0 & 0 & 0 & 1 & 0 & 0 & 0 & 0 & 0 & 0 \\ 0 & 0 & 0 & 0 & 0 & 0 & 0 & 1 & 0 & 0 & 0 & 0 \\ 0 & 0 & 0 & 0 & 0 & 0 & 1 & 0 & 0 & 0 & 0 & 0 \\ 0 & 0 & 0 & 0 & 0 & 0 & 0 & 0 & 1 & 0 & 0 & 0 \\ 0 & 0 & 0 & 0 & 0 & 0 & 0 & 0 & 0 & 1 & 0 & 0 \\ 0 & 0 & 0 & 0 & 0 & 0 & 0 & 0 & 0 & 0 & 1 & 0 \\ 0 & 0 & 0 & 0 & 0 & 0 & 0 & 0 & 0 & 0 & 0 & 1 \end{bmatrix}.$$

References

[1] G.H. Koo, Y.S. Park, Vibration analysis of a 3-dimensional piping system conveying fluid by wave approach, *International Journal of Pressure Vessels and Piping* 67 (1996) 249–256.
[2] G.H Koo, Y.S. Park, Vibration reduction by using periodic supports in a piping system, *Journal of Sound and Vibration* 210 (1998) 53–68.
[3] S.V. Sorokin, O.A. Ershova, Analysis of the energy transmission in compound cylindrical shell with and without internal heavy fluid loading by boundary integral equations and by Floquet theory, *Journal of Sound and Vibration* 291 (2006) 81–99.
[4] M.G. Kang, The influence of rotary inertia of concentrated masses on the natural vibrations of fluid-conveying pipes, *Journal of Sound and Vibration* 238 (2000) 179–187.
[5] S.Y. Lee, C.D. Mote Jr., A generalized treatment of the energetic of translating continua, part II: beams and fluid conveying pipes, *Journal of Sound and Vibration* 204 (1997) 735–753.
[6] S.S. Chen, Vibration and stability of a uniformly curved tube conveying fluid, *JASA* 51 (1972) 223–232.
[7] R.W. Doll, C.D. Mote, On the dynamic analysis of curved and twisted cylinders transporting fluids, *Journal of Pressure Vessel Technology* 98 (1976) 143–150.
[8] S. Gopalakrishnan, M. Martin, J.F. Doyle, A matrix methodology for spectral analysis of wave propagation in multiple connected timoshenko beams, *Journal of Sound and Vibration* 158 (1) (1992) 11–24.
[9] M.S. Kushwaha, P. Halevi, L. Dobrzynski, et al., Acoustic band structure of periodic elastic composites, *Physical Review Letters* 71 (1993) 2022–2025.
[10] M.S. Kushwaha, P. Halevi, G. Martinez, L. Dobrzynski, B. Djafari-Rouhani, Theory of acoustic band structure of periodic elastic composites, *Physical Review B* 49 (1994) 2313–2322.
[11] M.M. Sigalas, E.N. Economou, Elastic and acoustic wave band structure, *Journal of Sound and Vibration* 158 (1992) 377–382.
[12] Z. Liu, X. Zhang, Y. Mao, Y.Y. Zhu, Z. Yang, C.T. Chan, P. Sheng, Locally resonant sonic materials, *Science* 289 (2000) 1734–1736.
[13] C. Goffaux, J. Sánchez-Dehesa, A. Levy Yeyati, P. Lambin, A. Khelif, J.O. Vasseur, B. Djafari-Rouhani, Evidence of Fano-like interference phenomena in locally resonant materials, *Physical Review Letters* 88 (2002) 225502.
[14] M. Hirsekorn, P.P. Delsanto, N.K. Batra, P. Matic, Modelling and simulation of acoustic wave propagation in locally resonant sonic materials, *Ultrasonics* 42 (2004) 231–235.
[15] Z. Liu, C.T. Chan, P. Sheng, Three-component elastic wave band-gap material, *Physical Review B* 65 (2002) 165116.
[16] J.H. Wen, G. Wang, D.L. Yu, et al., Theoretical and experimental investigation of flexural wave propagation in straight beams with periodic structures: application to a vibration isolation structure, *Journal of Applied Physics* 97 (2005) 114907.
[17] D.L. Yu, Y.Z. Liu, J. Qiu, G. Wang, H.G. Zhao, Complete flexural vibration band gaps in membrane-like lattice structures, *Physics Letters A* 357 (2006) 154–158.

[18] D.L. Yu, Y.Z. Liu, H.G. Zhao, G. Wang, J. Qiu, Flexural vibration band gaps in Euler–Bernoulli beams with two-degree-of-freedom locally resonant structures, *Physical Review B* 73 (2006) 064301.
[19] X.S. Wen, *Photonic/Phononic Crystals Theory and Technology [M]*, Science Press, Beijing, 2006.
[20] D. Yu, J. Wen, H. Zhao, Y. Liu, X. Wen, Vibration reduction by using the idea of phononic crystals in a pipe-conveying fluid, *Journal of Sound and Vibration* 318 (2008) 193.
[21] M.W. Lesmez, Modal Analysis of Vibrations in Liquid-filled Piping System, PhD, Michigan State University, 1989.